

Secure Offloading in NOMA-Aided Aerial MEC Systems Based on Deep Reinforcement Learning

Hongjiang Lei, Mingxu Yang, Jiacheng Jiang, Ki-Hong Park, and Gaofeng Pan

Abstract—Mobile edge computing (MEC) technology can reduce user latency and energy consumption by offloading computationally intensive tasks to the edge servers. Unmanned aerial vehicles (UAVs) and non-orthogonal multiple access (NOMA) technology enable the MEC networks to provide offloaded computing services for massively accessed terrestrial users conveniently. However, the broadcast nature of signal propagation in NOMA-based UAV-MEC networks makes it vulnerable to eavesdropping by malicious eavesdroppers. In this work, a secure offload scheme is proposed for NOMA-based UAV-MEC systems with the existence of an aerial eavesdropper. The long-term average network computational cost is minimized by jointly designing the UAV’s trajectory, the terrestrial users’ transmit power, and computational frequency while ensuring the security of users’ offloaded data. Due to the eavesdropper’s location uncertainty, the worst-case security scenario is considered through the estimated eavesdropping range. Due to the high-dimensional continuous action space, the deep deterministic policy gradient algorithm is utilized to solve the non-convex optimization problem. Simulation results validate the effectiveness of the proposed scheme.

Index Terms—Mobile edge computing, unmanned aerial vehicle, physical layer security, non-orthogonal multiple access, deep reinforcement learning.

I. INTRODUCTION

A. Background and Related Works

MOBILE edge computing (MEC) enables offloading computation and storage resources to the network edge, allowing for task processing closer to where data is generated, thereby reducing data transmission latency and bandwidth requirements on Internet of Things (IoT) systems [1]-[3]. However, there remains a challenging issue for terminal devices located in remote areas or mountainous regions, as they need more infrastructure coverage to access reliable MEC servers. In such circumstances, due to the absence of MEC support and infrastructure limitations, terminal devices face significant restrictions and limitations in terms of computational and communication capabilities. Through the establishment of line of sight (LoS) connections with devices used by ground

Manuscript received.

This work was supported by the National Natural Science Foundation of China under Grant 62171031 and 61971080. (Corresponding author: *Jiacheng Jiang, Gaofeng Pan*.)

Hongjiang Lei, Mingxu Yang, and Jiacheng Jiang are with the School of Communications and Information Engineering, Chongqing University of Posts and Telecommunications, Chongqing 400065, China (e-mail: leihj@cqupt.edu.cn, ymx13648245248@163.com, cquptjhc@163.com).

Ki-Hong Park is with the CEMSE Division, King Abdullah University of Science and Technology (KAUST), Thuwal 23955-6900, Saudi Arabia (e-mail: khong.park@kaust.edu.sa).

Gaofeng Pan is with the School of Cyberspace Science and Technology, Beijing Institute of Technology, Beijing 100081, China (e-mail: gaofeng.pan.cn@ieee.org).

users (GUs), unmanned aerial vehicles (UAVs) can serve as “aerial MEC servers”, offering significant offloading services characterized by minimal network overhead and execution latency [4]. In Ref. [5], the total delay of all users was reduced by optimizing the scheduling variables, task offload ratio, and trajectory of the UAV. Furthermore, a novel penalty dual decomposition (PDD) algorithm was developed using the augmented Lagrangian method to solve the non-convex problem with mixed integers. The energy consumption of the UAV was reduced by optimizing the CPU frequencies, the amount of offloading, the transmission power, and the UAV’s trajectory. To address the non-convex problem, Liu *et al.* proposed the successive convex approximation (SCA)-based and the decomposition and iteration-based algorithms in their work [6]. The energy efficiency was also minimized in the scenarios where the UAV operated in both 1D and 2D trajectories [7]. In Ref. [8], the MEC system’s energy consumption was minimized by simultaneously optimizing the UAV’s beamforming vectors, CPU frequency, trajectory, and the GUs’ transmission power. An iterative algorithm featuring three stages was introduced to address the intricacies of the resultant non-convex optimization problem, each stage is solved by SCA, the semi-definite programming (SDP) and alternating optimization (AO) algorithms respectively. In Ref. [9], the authors maximized the weighted computation efficiency by concurrently optimizing task assignment, UAV’s trajectory, CPU frequency, and power allocation and proposed an alternative algorithm based on the Dinkelbach method, Lagrange duality, and SCA technique. Ref. [10] investigated the 3D trajectory and resource allocation optimization scheme in space-air-ground integrated networks, in which UAVs acted as MEC servers to provide computing services to GUs, and tasks that the UAVs cannot process were offloaded to the satellite for computation.

Nonorthogonal multiple access (NOMA) offers the advantage of improved spectral efficiency and increased system capacity by allowing multiple users to share the same time-frequency resources and has been extensively used in aerial MEC networks to reduce the latency and energy cost [11]-[14]. In Ref. [11], the weighted energy consumptions of the aerial MEC systems with orthogonal multiple access (OMA) and NOMA schemes were minimized through the joint optimization of the computation resource allocation and UAV trajectory. In Ref. [12], the total energy consumption was minimized by joint designing the task allocation, time scheduling, transmit power, and UAV trajectory. The nonlinear optimization problem was divided into two subproblems and was solved by the iterative algorithm. Zhang *et al.* [13] studied

the energy-efficient multiple UAVs-assisted MEC networks and minimized the weighted system energy consumption by jointly optimizing the radio and computation resources. In Ref. [14], the hybrid beamforming and NOMA techniques were utilized in the UAV-MEC networks to enhance the computation performance. The total computation rate of all the GUs was maximized by optimizing the UAV's three-dimensional (3D) position, hybrid beamforming design, and computational resource allocation. Two novel algorithms were introduced to deal with the non-convex optimization challenges for partial and binary offloading scenarios.

The broadcast nature of wireless channels allows eavesdroppers to also benefit from the LoS link provided by the UAV-MEC communication system, which makes user offloading information easy to intercept by terrestrial eavesdroppers [15]-[17] and aerial eavesdroppers [18]-[21]. Authors in Ref. [15] studied the secrecy performance of a dual-UAV-assisted MEC system with time division multiple access (TDMA) and NOMA schemes, wherein one UAV was utilized as the "aerial MEC server" and the other utilized as the friendly jammer to fight with the terrestrial eavesdroppers. The minimum secrecy computing capacity was maximized by jointly optimizing computation resources and UAVs' trajectories and an algorithm based on block coordinate descent (BCD) was introduced to handle the formulated problem. Ref. [16] investigated the security performance of a UAV-MEC system in the presence of multiple location-uncertain terrestrial eavesdroppers, where the aerial user offloaded data to multiple terrestrial MEC servers. The worst average secrecy capacity was maximized by jointly designing the UAV trajectory and transmit power, the power of artificial noise (AN) and the local computation ratio. Mao *et al.* investigated the robustness and security of multi-antenna aerial MEC networks in [17]. Considering the imperfect channel state information (CSI) during information offloading, the energy consumption of a multi-antenna UAV-assisted MEC network was minimized by jointly optimizing offloading time, beamforming vectors, CPU frequency, UAV's trajectory, and transmit power. Zhou *et al.* [18] investigated the security, latency, and offloading performance of the aerial MEC systems and this study revealed a tradeoff between the security and execution delay for the aerial MEC systems. To weaken the eavesdropping capability of flying eavesdroppers, the terrestrial jammer was employed to enhance the security of aerial MEC systems with TDMA scheme [19], [20], and NOMA scheme [21]. The minimum average secrecy capacity was maximized by optimizing the resources and trajectory of the aerial MEC server, respectively.

Considering the intricacy of task scheduling and resource allocation in UAV-MEC networks and the uncertainty of the environment, traditional optimization methods based on the SCA and BCD technologies are generally complicated to solve the formulated non-convex problems. Deep reinforcement learning (DRL) has been widely applied to solve dynamic decision-making problems in recent years [22]-[24]. In [25], the consumed energy of all GUs was minimized by optimizing the UAVs' trajectory, user scheduling, and computation resources. An algorithm formulated on convex optimization principles and another algorithm based on DRL were proposed

to address it iteratively and facilitate fast decision-making. To guarantee load fairness among UAVs, a 3D multi-UAV trajectory optimization scheme was investigated in Ref. [26], wherein the GU selected the optimal UAV for task offloading and the formulated problem was solved by utilizing the deep deterministic policy gradient (DDPG) algorithm. Ref. [27] proposed a novel optimization framework wherein the latency, energy, and price in different combinations according to users' requirements, and a deep Q-network (DQN) based algorithm was proposed to deal with the offloading optimization problem. A secure model for transmission in the multiple UAV-MEC network was considered in [28], wherein the spiral placement algorithm was utilized to minimize the required server UAVs for full GUs coverage and two secure transmission schemes based on reinforcement learning were proposed to maximize the weighted delay and the residual energy utility. TABLE I presents typical works related to aerial MEC systems.

B. Motivation and Contributions

Although the UAV-MEC system has been extensively investigated, the in-depth research and analysis in this field still need to be improved. The scenarios involving location-uncertain eavesdropping and ensuring secure transmission of offloading data still need to be explored. This work aims to ensure the security of user data transmission and computation efficiency while comprehensively considering eavesdropping location uncertainty. The main contributions of this work can be summarised as follows.

- 1) With the premise of ensuring secure offloading in a NOMA-aided aerial MEC system, we propose a new optimization scheme to minimize average computational cost by jointly designing the 3D trajectory of the UAV, the user's transmit power, and CPU frequency. To cope with the high-dimensional and continuous action space control problem in the UAV-MEC scenario, a DDPG-based trajectory and dynamic resource allocation (TDRA) scheme is proposed to solve the presented optimization challenge and obtain effective user resource allocation and UAV flight trajectory design.
- 2) Relative to [18], [19], [21], wherein 2D trajectory was jointly designed with transmit power and other parameters to obtain the security offloading in the UAV-MEC system with a location-uncertain eavesdropper. This work minimizes the average network computational cost by jointly designing the UAV's 3D trajectory, GUs' transmit power and computational frequency while ensuring the security of GUs' offloaded data. A DDPG-based TDRA scheme is proposed to solve the formulated problems.
- 3) Relative to [10], [24], [25], [26] wherein 3D trajectory of the UAV was designed to optimize the energy efficiency of aerial MEC systems with OMA scheme, we design 3D trajectory of the UAV to minimize the average network computational cost of aerial MEC systems with NOMA scheme while considering security constraint. The worst-case security scenario with the eavesdropper's

TABLE I: Recent Works on Aerial MEC Systems

Reference	Optimization Objective	UAV Trajectory	MA Scheme	PLS	Aerial E	Imperfect Location of E	Method
[5]	Delay	2D	TDMA				PDD
[6], [7]	UAV consumed energy	2D	TDMA				SCA
[8]	User and UAV consumed energy	2D	TDMA				SCA, SDP, AO
[9]	Energy efficiency	2D	FDMA				Dinkelbach, SCA
[10]	Energy efficiency	3D	TDMA				Dinkelbach, BCD
[13]	User and UAV consumed energy	2D	NOMA				SCA
[15]	Secrecy capacity	2D	NOMA	✓			BCD
[17]	User and UAV consumed energy	2D	TDMA	✓			SCA
[18]	Secrecy capacity	Fixed ^a	NOMA	✓	✓	✓	BCD, SCA
[19]	Secrecy capacity	2D	TDMA	✓	✓		BCD, SCA
[20]	Secrecy capacity	2D	TDMA	✓	✓		Double DQN
[21]	Secrecy capacity	2D	NOMA	✓	✓	✓	BCD, SCA
[24]	Energy efficiency	3D	TDMA				DQN
[25]	User consumed energy	3D	FDMA				BCD, DDPG
[26]	User and UAV consumed energy	3D	TDMA				DDPG
[27]	User computing cost	Fixed ^a	FDMA	✓	✓		DQN
[28]	System utility	Fixed ^a	TDMA	✓	✓		Nash Q-learning
Our work	User delay and consumed energy	3D	NOMA	✓	✓	✓	DDPG

Fixed^a: The UAV hovers in a fixed position.

TABLE II: Notation and Symbols

Notation	Description
$\mathbf{q}_S(n)$	Location of S in the n th slot
$\mathbf{q}_E(n)$	Location of E in the n th slot
$\tilde{\mathbf{q}}_E$	Centre of E estimated location
\mathbf{w}_J	Location of J
$\mathbf{w}_{U_k}(n)$	Location of U_k in the n th slot
δ_t	Time slot size
$v(n)$	The velocity of S
$\theta(n)$	The polar angle of S
$\varphi(n)$	The azimuthal angle of S
$p_k(n), P_J$	Transmit power of U_k and J
P_k^{\max}	Peak transmit power of U_k
B	Channel bandwidth
σ_S^2, σ_E^2	The power of AWGN at S and E
$f_k(n)$	CPU frequency of U_k
F_k^{\max}, F_S^{\max}	Peak CPU frequency of U_k and S
$L_k(n)$	The remaining data of U_k
C_k, C_S	CPU cycles required for U_k and S to compute each bit task data
φ_k, φ_S	The effective capacitance coefficient of U_k and S
$E_S(n)$	The residual energy of S
w_1, w_2	The weighted factor of energy consumption and execution delay
c_E, c_T	Per unit cost of energy consumption and execution delay
Z_{\min}, Z_{\max}	Flight altitude range of S

location uncertainty is considered through the estimated eavesdropping region.

C. Organization

The subsequent sections are structured as follows. Section II presents the system model and gives the corresponding optimization problem. Section III provides a detailed description of the DDPG-based TDRA scheme and gives the definitions related to DRL. Section IV provides simulation results and analysis. Finally, the paper is summarized in Section V. The notations and symbols used in this work are listed in TABLE II.

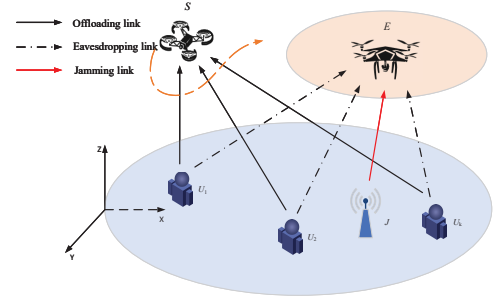


Fig. 1: System model.

II. SYSTEM MODEL AND PROBLEM FORMULATION

Fig. 1 shows the considered aerial MEC system, which consists of an aerial MEC server (S), K GUs U_k , denoted by the set $\mathcal{K} = \{1, 2, \dots, K\}$, and an aerial malicious eavesdropper (E). A terrestrial friendly jammer (J) is utilized to mitigate the eavesdropping capabilities of E by transmitting artificial noise (AN). All nodes are presumed to operate in half-duplex mode and are equipped with a single antenna. The total flight time of S is represented as T , which is equally divided into N slots, and each slot with a duration of $\delta_t = \frac{T}{N}$. Assume δ_t is small enough for treating the positions of S as constant in each slot [29].

A 3D Cartesian coordinate is utilized and the location of S is expressed as $\mathbf{q}_S(n) = [x_S(n), y_S(n), z_S(n)]^T$. The coordinates of J and U_k at the n th slot are represented as $\mathbf{w}_J = [x_J, y_J]^T$ and $\mathbf{w}_{U_k} = [x_k, y_k]^T$, respectively. It is assumed that E works at a certain altitude¹ of z_E and its exact location is unavailable for S and J [30]. Like [18], [21], E lies in a circle with center $\tilde{\mathbf{q}}_E = [\tilde{x}_E, \tilde{y}_E]^T$

¹The aerial eavesdropper is assumed to be a malicious eavesdropper that passes through certain areas that contain sensitive signals. In particular, the aerial eavesdroppers could be disguised as a civilian aircraft and work at a fixed altitude. Considering the more practical scenario of E working in a 3D trajectory is an interesting work and will be part of future work.

and radius r_E , which satisfies $\|\mathbf{q}_E(n) - \tilde{\mathbf{q}}_E\| \leq r_E$, where $\mathbf{q}_E(n) = [x_E(n), y_E(n)]^T$ denotes the exact location of E .

A. Secure Communication Model

The ground-to-air (G2A) link between U_k and u ($u \in \{S, E\}$) is assumed to be a probabilistic LoS link and the probability is expressed as [31]²

$$P_{k,u}^{\text{LoS}}(n) = \frac{1}{1 + \eta_a \exp\left(-\eta_b \left(\frac{\pi}{180} \arcsin\left(\frac{z_u(n)}{d_{k,u}(n)}\right) - \eta_a\right)\right)}, \quad (1)$$

where $d_{k,u}(n) = \sqrt{z_u(n)^2 + \|[\mathbf{x}_u(n), \mathbf{y}_u(n)]^T - \mathbf{w}_{U_k}\|^2}$, η_a and η_b are environment parameters, and $z_u(n)$ denotes the altitude of u . The average path loss between U_k and u in dB is expressed as [31]

$$L_{k,u}(n) = P_{k,u}^{\text{LoS}}(n) L_{k,u}^{\text{LoS}}(n) + P_{k,u}^{\text{NLoS}}(n) L_{k,u}^{\text{NLoS}}(n), \quad (2)$$

where $P_{k,u}^{\text{NLoS}}(n) = 1 - P_{k,u}^{\text{LoS}}(n)$, $L_{k,u}^{\text{LoS}}(n) = L_{k,u}^{\text{FS}}(n) + \eta_{\text{LoS}}$ and $L_{k,u}^{\text{NLoS}}(n) = L_{k,u}^{\text{FS}}(n) + \eta_{\text{NLoS}}$ represent the pathloss of LoS and NLoS links in dB between U_k and u , respectively, $L_{k,u}^{\text{FS}}(n) = 20\log_{10}d_{k,u}(n) + 20\log_{10}\left(\frac{4\pi f_c}{c}\right)$ is free space pathloss, f_c is the carrier frequency, c denotes the velocity of light, η_{LoS} and η_{NLoS} represent the excessive pathloss for LoS and NLoS links, respectively. The channel gain between U_k and u at the n th slot is expressed as

$$h_{k,u}(n) = 10^{-\frac{L_{k,u}(n)}{10}}. \quad (3)$$

NOMA-based UAV-MEC systems not only can attain higher spectral efficiency and ensure the fairness of user offloading through the power allocation mechanism but also effectively can reduce the delay and energy consumption of user offloading [33]. Thus, it is assumed that users offload data to S with NOMA technology. In particular, S utilizes channel state information (CSI)-based successive interference cancellation (SIC) technology to decode user information in descending order of channel gain [34]-[36]. The signal-to-interference-plus-noise-ratio (SINR) of the signal from U_k at S is expressed as

$$\begin{aligned} \gamma_{k,S}(n) &= \frac{h_{k,S}(n) p_k(n)}{h_{J,S}(n) P_J + \sum_{l \neq k, l \in \mathcal{K}} \lambda_{k,l}(n) h_{l,S}(n) p_l(n) + \sigma_S^2} \\ &\stackrel{(a)}{=} \frac{h_{k,S}(n) p_k(n)}{\sum_{l \neq k, l \in \mathcal{K}} \lambda_{k,l}(n) h_{l,S}(n) p_l(n) + \sigma_S^2}, \forall k, n, \end{aligned} \quad (4)$$

where $h_{i,S}(n)$ is the channel gain between U_i and S , $i \in \{k, l\}$, $p_i(n)$ denotes the transmit power of U_i , σ_S^2 represents the additive white Gaussian noise (AWGN) power at S , step

²In Ref. [32], the average rate with different 3D trajectories was compared, and the results demonstrated that there is an optimal 3D trajectory to maximize the average rate, which is one of the motivations of this work.

(a) holds if the friendly jammer is considered³, and $\lambda_{k,l}(n)$ indicates the relationship between the channel gains of U_k - S and U_l - S in the n th slot, which is defined as [15], [21]

$$\lambda_{k,l}(n) = \begin{cases} 1, & L_{k,S}(n) < L_{l,S}(n), \\ 0, & L_{k,S}(n) \geq L_{l,S}(n). \end{cases} \quad (5)$$

Specifically, $\lambda_{k,l}(n) = 1$ signifies that U_k - S link has higher channel quality than U_l - S link, and $\lambda_{k,l}(n) + \lambda_{l,k}(n) = 1$. Therefore, the instantaneous offloading rate from U_k at S is written as

$$R_{k,S}(n) = B \log_2 (1 + \gamma_{k,S}(n)), \quad (6)$$

where B is the channel bandwidth.

Similarly, the instantaneous offloading rate from U_k at E is expressed as

$$R_{k,E}(n) = B \log_2 (1 + \gamma_{k,E}(n)), \quad (7)$$

where $\gamma_{k,E}(n) = \frac{h_{k,E}(n) p_k(n)}{h_{J,E}(n) P_J + \sum_{z \in \mathcal{K}_k} h_{z,E}(n) p_z(n) + \sigma_E^2}$, $\mathcal{K}_k = \{U_z | L_{z,E}(n) \geq L_{k,E}(n)\}$ denotes the set whose channel gain is worse than the channel gain between U_k and E , $h_{z,E}(n)$ is the channel gain between U_z and E , $h_{J,E}(n)$ is the channel gain between J and E , P_J is the transmit power of J , and σ_E^2 represents the AWGN power at E .

Due to the uncertainty in the position of E , the exact value of $R_{k,E}(n)$ cannot be obtained [18], [21]. To facilitate the analysis, we consider the eavesdropping rate $R_{k,E}^{\text{ub}}(n)$ in the worst-case security situation. By using the triangle inequality to scale the distance, the lower bound of the Euclidean distance between U_k and E is expressed as

$$\begin{aligned} d_{k,E} &= \sqrt{z_E^2 + (\|\mathbf{w}_{U_k}(n) - \mathbf{q}_E(n)\|)^2} \\ &\geq \sqrt{z_E^2 + (\|\mathbf{w}_{U_k}(n) - \tilde{\mathbf{q}}_E\| - \|\tilde{\mathbf{q}}_E - \mathbf{q}_E(n)\|)^2} \\ &\geq \sqrt{z_E^2 + (\|\mathbf{w}_{U_k}(n) - \tilde{\mathbf{q}}_E\| - r_E)^2} \triangleq d_{k,E}^{\text{lb}}. \end{aligned} \quad (8)$$

Similarly, the upper bound of the distance between J , U_z ($z \in \mathcal{K}_k$) and E are expressed as

$$\begin{aligned} d_{J,E} &= \sqrt{z_E^2 + (\|\mathbf{w}_J - \mathbf{q}_E(n)\|)^2} \\ &\leq \sqrt{z_E^2 + (\|\mathbf{w}_J - \tilde{\mathbf{q}}_E\| + \|\tilde{\mathbf{q}}_E - \mathbf{q}_E(n)\|)^2} \\ &\leq \sqrt{z_E^2 + (\|\mathbf{w}_J - \tilde{\mathbf{q}}_E\| + r_E)^2} \triangleq d_{J,E}^{\text{ub}} \end{aligned} \quad (9)$$

and

$$\begin{aligned} d_{z,E} &= \sqrt{z_E^2 + (\|\mathbf{w}_{U_z}(n) - \mathbf{q}_E(n)\|)^2} \\ &\leq \sqrt{z_E^2 + (\|\mathbf{w}_{U_z}(n) - \tilde{\mathbf{q}}_E\| + \|\tilde{\mathbf{q}}_E - \mathbf{q}_E(n)\|)^2} \\ &\leq \sqrt{z_E^2 + (\|\mathbf{w}_{U_z}(n) - \tilde{\mathbf{q}}_E\| + r_E)^2} \triangleq d_{z,E}^{\text{ub}}, \end{aligned} \quad (10)$$

³It is assumed that the AN signals emitted by J conform to a Gaussian pseudo-random sequence since both S and J belong to a legitimate network. Specifically, S has prior knowledge of the AN sent by J and the AN signals can be ideally removed from the received signals at S . Because E does not belong to the legitimate network, it is not aware of the existence of J and treats all signals eavesdropped as the user's signals. Therefore, the AN signal sent by J will interfere with E [15], [20], [21], [37], [38].

respectively. Then we obtain

$$\begin{aligned} R_{k,E}^{\text{ub}}(n) &= B \log_2 \left(1 + \gamma_{k,E}^{\text{ub}}(n) \right) \\ &= B \log_2 \left(1 + \frac{h_{k,E}^{\text{ub}}(n) p_k(n)}{h_{J,E}^{\text{lb}}(n) P_J + \sum_{z \in \mathcal{K}_k} h_{z,E}^{\text{lb}}(n) p_z(n) + \sigma_E^2} \right), \end{aligned} \quad (11)$$

where the superscript ‘ub’ and ‘lb’ signify the upper and lower bounds, $h_{k,E}^{\text{ub}}$, $h_{J,E}^{\text{lb}}$, and $h_{z,E}^{\text{lb}}$ are obtained by substituting $d_{k,E}^{\text{lb}}$, $d_{J,E}^{\text{ub}}$, and $d_{z,E}^{\text{ub}}$ into (1), (2), and (3), respectively.

The worst instantaneous secrecy offloading rate of U_k in n th slot is expressed as

$$R_k^{\text{sec}}(n) = [R_{k,S}(n) - R_{k,E}^{\text{ub}}(n)]^+, \quad (12)$$

where $[x]^+ = \max\{x, 0\}$. To prevent E from eavesdropping, the following condition should be met [38], [39]

$$R_k^{\text{sec}}(n) \geq R_{\min}^{\text{sec}}, \forall k, n, \quad (13)$$

where R_{\min}^{sec} denotes the threshold secure offloading rate.

B. Mobile Edge Computing Model

It is assumed that U_k has the computationally-intensive and latency-sensitive task L_k which needs to be completed within the flying time T , where L_k represents the total amount of task data. The computing tasks can not be finished locally due to the users’ limited computing resources and battery capacity. To solve this problem, users can offload part of the computational tasks to the aerial edge server for processing. Note that the computational tasks are bitwise independent and can be randomly separated to enable parallel computation between local execution and task offloading [8], [11].

1) *Local Computation*: To fully utilize the power of local computing, U_k and S always adopt a dynamic voltage and frequency scaling technology [9]. Therefore, the CPU frequency of U_k is adjusted to reduce the energy consumed to perform local computation. The amount of locally computed data and energy consumption for U_k in the n th slot is given by

$$L_k^{\text{loc}}(n) = \frac{\delta_t f_k(n)}{C_k}, \forall k, n, \quad (14a)$$

$$E_k^{\text{loc}}(n) = \delta_t \varphi_k f_k^3(n), \forall k, n, \quad (14b)$$

where C_k denotes the CPU cycles required to compute 1-bit task, $f_k(n)$ is the CPU frequency of U_k , and φ_k is the effective capacitance of U_k , depending on the U_k ’s chip architecture [7].

2) *Computation Offloading*: The amount of offloaded data from U_k and the energy consumption for transmission at U_k is denoted as

$$L_k^{\text{off}}(n) = \delta_t R_k^{\text{sec}}(n), \forall k, n, \quad (15a)$$

$$E_k^{\text{off}}(n) = p_k(n) \delta_t, \forall k, n. \quad (15b)$$

The CPU frequency and energy to process U_k ’s offloading data at S is expressed as [15], [21]

$$f_{Sk}(n) = \frac{L_k^{\text{off}}(n) C_S}{\delta_t}, \forall k, n, \quad (16a)$$

$$E_{S,k}^{\text{com}}(n) = \delta_t \varphi_S f_{Sk}^3(n), \forall k, n, \quad (16b)$$

where C_S and φ_S signify the CPU cycles required by S to compute 1-bit of data and the effective capacitance of S , respectively. At each slot, the sum of the amount of offloaded data must be less than that S can deal with, which is expressed as

$$\sum_{k=1}^K f_{Sk}(n) \leq F_S^{\max}, \forall n, \quad (17)$$

where F_S^{\max} is the maximum computational frequency of S .

The consumed propulsion energy of S in n th slot is expressed as [40]

$$E_S^{\text{fly}}(n) = P_v(n) \delta_t, \forall n, \quad (18)$$

where $P_v(n) = P_i \left(\sqrt{1 + \frac{v^4(n)}{4v_0^4}} - \frac{v^2(n)}{2v_0^2} \right)^{\frac{1}{2}} + \frac{1}{2} d_0 \rho s A v^3(n) + P_0 \left(1 + \frac{3v^2(n)}{U_{tip}^2} \right)$ is the propulsion power consumption of rotary-wing UAV S , where P_0 and P_i denote the blade profile and the induced power in hover state, U_{tip} signifies the tip velocity of the rotor blade, v_0 denotes the mean rotor induced speed in hover, d_0 , ρ , s and A represent the drag ratio of the fuselage, the air density, solidity of the rotor and rotor disc area, respectively.

Based on [41], we only take into account the energy consumption of the propulsion and computation for executing user offloading tasks, while disregarding the energy consumption related to communication, which represents merely a small fraction of the UAV’s total energy usage. Thus, the residual energy of S in n th slot is expressed as

$$E_S(n) = E_S^{\max} - \sum_{i=0}^{n-1} \left(\sum_{k=1}^K (E_{S,k}^{\text{com}}(i) + E_S^{\text{fly}}(i)) \right), \quad (19)$$

where E_S^{\max} denotes the battery capacity of S . To ensure that all U_k ’s tasks can be finished before S runs out of the given energy, the following condition must be satisfied

$$E_S(N) \geq E_S^{\min}, \quad (20)$$

where E_S^{\min} denotes the minimum energy that ensure S can fly directly back to the specified final position after the completion of the mission.

3) *Computation Cost*: Similar to [25], [27], [28], the delay and energy consumption in returning processed results are neglected because of the substantial difference in transmitting power between S and U_k and the considerably smaller data volume generated by task calculation results than that caused by U_k . When the computational tasks of all the GUs are completed, the energy consumption of the considered system is obtained as

$$E_c = \sum_{n=1}^N \sum_{k=1}^K (E_k^{\text{loc}}(n) + E_k^{\text{off}}(n)). \quad (21)$$

$T_k(n)$ is defined as the state of U_k ’s remaining unprocessed data in the n th slot, which is given as

$$T_k(n) = \begin{cases} 1, & \text{if } L_k(n) > 0, \\ 0, & \text{otherwise,} \end{cases} \quad (22)$$

where $L_k(n)$ denotes the remaining data of U_k in the n th slot, which is modeled as

$$L_k(n) = [L_k(n-1) - (L_k^{\text{loc}}(n-1) + L_k^{\text{off}}(n-1))]^+. \quad (23)$$

Note that $L_k[0] = L_k$ is satisfied. Then the delay of U_k is $T_k = \delta_t \sum_{n=1}^{N_k} T_k(n)$, where N_k is the total slots for U_k to process L_k . The latency of all users in the system is

$$T_c = \sum_{k=1}^K T_k. \quad (24)$$

Finally, the average computation cost, the weighted energy consumption and execution delay, is defined as [21]

$$U_c = \frac{1}{K} (\omega_1 c_E E_c + \omega_2 c_T T_c), \quad (25)$$

where c_E and c_T denote the unit costs for energy consumption and time delay, respectively, $\omega_1 \in [0, 1]$ and $\omega_2 \in [0, 1]$ are the weighting factors satisfying $\omega_1 + \omega_2 = 1$, which determine the priority or importance on energy consumption and time delay.

C. Problem Formulation

In this work, the average computation cost of the considered system is minimized by jointly designing the S 's trajectory, U_k 's transmit power, and CPU frequency. Let $\mathbf{Q} = \{\mathbf{q}_S(n), \forall n\}$, $\mathbf{P} = \{p_k(n), \forall k, n\}$, and $\mathbf{F} = \{f_k(n), \forall k, n\}$. The optimization problem is expressed as

$$\mathcal{P}_1 : \min_{\mathbf{Q}, \mathbf{P}, \mathbf{F}} U_c \quad (26a)$$

$$\text{s.t. } \|\mathbf{q}_S(n+1) - \mathbf{q}_S(n)\| \leq V_S^{\max} \delta_t, \forall n, \quad (26a)$$

$$\|\mathbf{q}_S(n) - \mathbf{q}_E(n)\| \geq d_{\min}, \forall n, \quad (26b)$$

$$\mathbf{q}_S(0) = \mathbf{q}_S^I, \quad (26c)$$

$$Z_{\min} \leq z_S(n) \leq Z_{\max}, \forall n, \quad (26d)$$

$$0 \leq p_k(n) \leq P_k^{\max}, \forall k, n, \quad (26e)$$

$$0 \leq f_k(n) \leq F_k^{\max}, \forall k, n, \quad (26f)$$

$$\sum_{k=1}^K L_k(N) = 0, \quad (26g)$$

$$(5), (13), (17), (20),$$

where \mathbf{q}_S^I signifies the initial position of S , V_S^{\max} is the maximum speed of S , d_{\min} denotes the minimum safety distance, Z_{\min} and Z_{\max} denote the minimum and maximum altitude of S , respectively. (26a) represents the maximum flight speed constraint of S , (26b) denotes the minimum collision avoidance distance between S and E , (26c) is a constraint for the initial position of S , (26d) is the flight altitude constraint of S , (26e) denotes the constraint of transmit power of U_k , (26f) is the constraint of the CPU frequency of U_k and S , (5) denotes the constraint for decoding ability of U_k , and (26g) is constraint for ensuring computation tasks are completed.

The constraints (13) and (17) are non-convex because of the coupling of two optimization variables, \mathbf{Q} and \mathbf{P} . And the constraint (20) is also non-convex since the energy consumption model is involved. Furthermore, considering the vast solution

space for decision-making and the dynamic environmental changes resulting from the mobility of UAV, optimization problem \mathcal{P}_1 is challenging to solve using traditional convex optimization methods.

III. DDPG-BASED TRAJECTORY AND DYNAMIC RESOURCE ALLOCATION SCHEME

DRL technology can adapt to dynamic environments and excel at tackling various non-convex and highly complex problems. Therefore, to address the above mentioned issues, \mathcal{P}_1 is re-modeled as a single-agent extension of the Markov decision process (MDP), which is then solved by a DRL method as follows.

A. MDP Formulation

Like [42], [43], the spherical coordinate $\{v, \theta, \varphi\}$ is utilized to describe the velocity and direction of S , where v denotes the velocity, θ represents the polar angle from the positive z -axis, constrained within the range $0 \leq \theta \leq \pi$, while φ denotes the azimuthal angle in the xy -plane, measured from the x -axis and constrained within the range $0 \leq \varphi \leq 2\pi$. Then, the velocity is expressed as $\mathbf{v}(n) = \{v(n), \theta(n), \varphi(n)\}$. Define the distance of S within two consecutive slots as $v(n) \delta_t = \|\mathbf{q}_S(n+1) - \mathbf{q}_S(n)\|$, we have

$$x_S(n+1) = x_S(n) + v(n) \delta_t \sin \theta(n) \cos \varphi(n), \quad (27a)$$

$$y_S(n+1) = y_S(n) + v(n) \delta_t \sin \theta(n) \sin \varphi(n), \quad (27b)$$

$$z_S(n+1) = z_S(n) + v(n) \delta_t \cos \theta(n). \quad (27c)$$

At each slot, S determines its speed $v(n)$, flight direction $\theta(n)$ and $\varphi(n)$, the transmit power $p_k(n)$ and computational frequency $f_k(n)$ of each U_k to obtain the minimum average computational cost for system users. Since S 's movement will affect its environment, the users' total computational cost depends on the environment's current state and the UAV's actions. Furthermore, the previous state and actions of the UAV can together result in a new stochastic state of the environment.

As a result, \mathcal{P}_1 can be represented as a MDP, which is defined as a four-tuple $\langle \mathcal{S}, \mathcal{A}, \mathcal{P}, \mathcal{R} \rangle$, where \mathcal{S} , \mathcal{A} , \mathcal{P} , and \mathcal{R} denote the state space, action space, state transition probability, and reward, respectively, which are presented as follows.

1) *The state space (\mathcal{S}):* The state $s(n)$ is composed of $\mathbf{q}_S(n)$, $E_S(n)$, $R_k^{\text{sec}}(n)$ and $L_k(n)$, that is,

$$s(n) = \{\mathbf{q}_S(n), E_S(n), R_k^{\text{sec}}(n), L_k(n), \forall k\}. \quad (28)$$

2) *The action space (\mathcal{A}):* Since S is required to determine its movements including the flight speed $v(n)$, the polar angle $\theta(n)$, the azimuthal angle $\varphi(n)$, the U_k 's transmit power $p_k(n)$ and computational frequency $f_k(n)$. The action space $a(n)$ is designed by

$$a(n) = \{v(n), \theta(n), \varphi(n), p_k(n), f_k(n), \forall k\}. \quad (29)$$

The ranges of each element in $a(n)$ are expressed as, $v(n) \in [0, V_S^{\max}]$, $\theta(n) \in [0, \pi]$, $\varphi(n) \in [0, 2\pi]$, $p_k(n) \in [0, P_k^{\max}]$, and $f_k(n) \in [0, F_k^{\max}]$.

It can be observed that the state space \mathcal{S} has $(4 + 2K)$ dimensions, and the action space \mathcal{A} is a continuous set with

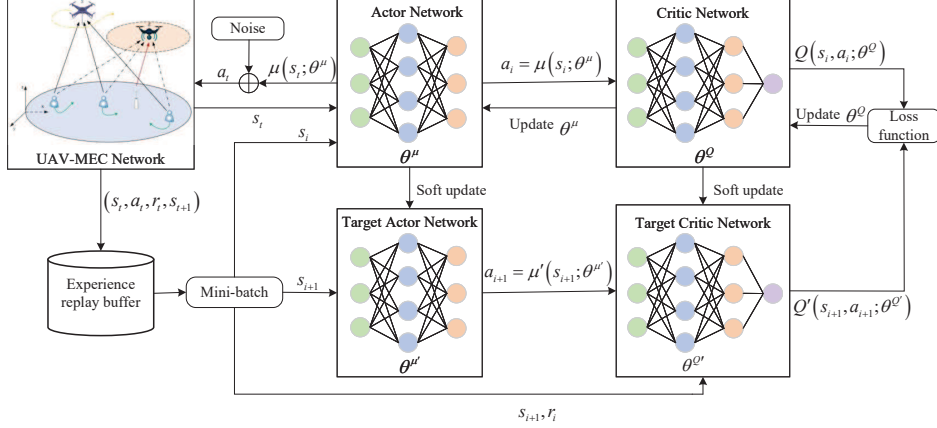


Fig. 2: DDPG framework in the UAV-MEC network.

$(3 + 2K)$ dimensions. Moreover, with increasing K , the size of \mathcal{S} and \mathcal{A} exponentially increases.

3) *The reward (\mathcal{R})*: According to the optimization problem (26), the reward of this work is designed by comprising the following components: the offloading data reward, the satisfying constraints reward, and the computational reward, which are introduced as follows.

- The offloading data reward: Since U_k can reduce their own computational costs by offloading tasks to S , the reward ($r_{\text{off}}(n)$) is designed as

$$r_{\text{off}}(n) = \kappa_f \delta_t \sum_{k=1}^K \vartheta_k(n) R_k^{\text{sec}}(n), \quad (30)$$

where κ_f denotes a positive constant utilized for the adjustment of $r_{\text{off}}(n)$ and ϑ is applied to control the reward gained from U_k , which is expressed as

$$\vartheta_k(n) = \begin{cases} 1, & \text{if } L_k(n) > 0, \\ 0, & \text{otherwise.} \end{cases} \quad (31)$$

- The satisfying constraints reward: To ensure the constraints of the optimization problem are satisfied, the satisfying constraints reward ($r_p(n)$) is designed as

$$r_p(n) = -\lambda_{\text{ac}}(n) \kappa_{\text{ac}} - \lambda_{\text{rc}}(n) \kappa_{\text{rc}} - \kappa_{\text{er}}(n), \quad (32)$$

where κ_{ac} and κ_{rc} denote the rewards related with the collision constraint (26b) and S 's computing resource constraints (17), respectively, $\lambda_{\text{ac}}(n)$ and $\lambda_{\text{rc}}(n)$ are binary coefficients, $\lambda_{\text{ac}}(n) = 1$ denotes (26b) is not satisfied, $\lambda_{\text{rc}}(n) = 1$ denotes (17) is not met, $\kappa_{\text{er}}(n)$ is a sparse reward to judge the data remaining of all U_k when S 's energy has been exhausted and defined as

$$\kappa_{\text{er}}(n) = \begin{cases} 0, & n = 1, \dots, N-1, \\ \zeta \sum_{k=1}^K L_k(N), & n = N, \end{cases} \quad (33)$$

where ζ is a positive constant that is used to adjust $\kappa_{\text{er}}(n)$. A negative reward will be given if constraint (26g) is not met; otherwise, no reward will be provided. It should be noted that all the terms in (32) always

be negative. This is because negative rewards imply punishment when constraints are not met.

Thus, the reward function in this work is expressed as

$$r(n) = r_{\text{off}}(n) + r_p(n) - U_c(n), \quad (34)$$

where $U_c(n)$ denotes the computation cost at the n th slot.

At each time step, S transitions from $s(n)$ to $s(n+1)$ based on $a(n)$ and \mathcal{P} , and then receives a reward $r(n)$. The sequential transitions $(s(n), a(n), r(n), s(n+1))$ are stored as experiences in a replay buffer and randomly sampled to train neural networks (NNs). Then S continuously selects the optimal action through the trained NN to maximize the cumulative discount reward.

B. DDPG-Based Trajectory and Dynamic Resource Allocation Scheme

Considering the high-dimensional continuous $a(n)$ of the formulated problem, the DDPG-based TDRA algorithm is proposed to address the above proposed MDP. The aim is to enable the agent to learn an optimal policy that maximizes the cumulative reward \mathcal{R}_n by jointly optimizing the policy and the value function networks, which is defined as [44]

$$\mathcal{R}_n = \sum_{n=0}^{N-1} \beta^n r(n), \quad (35)$$

where $\beta \in [0, 1]$ represents the discount factor, which determines the trade-off between current and future rewards.

As illustrated in Fig. 2, the DDPG-based TDRA algorithm is implemented with an actor-critic architecture containing an actor NN and a critic NN. The actor NN is inputted with the current environmental state $s(n)$ and then provides the corresponding action $a(n)$ to the NOMA-aided aerial MEC network based on the weight θ^μ of the actor NN and a stochastic noise \mathcal{N}_n , the instantaneous action $a(n)$ is given by [44]

$$a(n) = \mu(s(n); \theta^\mu) + \mathcal{N}_n, \quad (36)$$

where \mathcal{N}_n is exploratory random noise to increase action randomness and diversity and enable more effective state space exploration.

$$\begin{aligned}\nabla_{\theta^\mu} J &\approx E \left[\nabla_{\theta^\mu} Q(s, a; \theta^Q) \mid_{s=s(n), a=\mu(s(n); \theta^\mu)} \right] \\ &= E \left[\nabla_a Q(s, a; \theta^Q) \mid_{s=s(n), a=\mu(s(n))} \nabla_{\theta^\mu} \mu(s(n); \theta^\mu) \mid_{s=s(n)} \right]\end{aligned}\quad (37)$$

During training, \mathcal{N}_n decreases gradually, allowing the actor NN to transition from exploration to exploitation, effectively leveraging learned knowledge and experience. It is worth noting that $a(n)$ is constrained within the range $[0, 1]$. Therefore, it will be clipped if the noise-added action value exceeds the desired range. Subsequently, S executes the current action $a(n)$. The environment is transferred to the next state $s(n+1)$ according to a certain state transition probability. At the same time, the environment returns an immediate reward $r(n)$ to the agent according to the quality of $a(n)$.

To stabilize the training process and break the correlation of input data, S stores the current experience $(s(n), a(n), r(n), s(n+1))$ in the replay buffer \mathcal{B} with size M_r and randomly samples a mini-batch of M_b experience samples from \mathcal{B} to train the actor NN and the critic NN, to approximate the action function and the action-value function, respectively.

Furthermore, the pair $(s(n), a(n))$ will be fed into the critic NN to evaluate $a(n)$. The critic NN with weight θ^Q will output an estimated Q-value $Q(s(n), a(n); \theta^Q)$, where the Q-value is the expected long-term reward [44]. To enhance training stability and facilitate convergence, the DDPG-based TDRA algorithm incorporates target actor NN and target critic NN with weights $\theta^{\mu'}$ and $\theta^{Q'}$, respectively.

Based on the principle of the policy gradient theorem [44], the goal of the DDPG-based TDRA algorithm is to maximize the discounted cumulative reward $J(\mu)$. The weights θ^μ of the actor NN are updated along the direction of the gradient that improves the action-value $Q(s(n), a(n); \theta^Q)$, which is obtained as (37), shown at the top of next page.

The critic NN is updated to minimize the loss function $L(\theta^Q)$, which is defined as

$$L(\theta^Q) = (y_i - Q(s_i, a_i; \theta^Q))^2, \quad (38)$$

where y_i is the target Q-value output by the target critic NN, defined as

$$y_i = r_i + \beta Q(s_{i+1}, \mu'(s_{i+1}; \theta^{\mu'}); \theta^{Q'}). \quad (39)$$

In terms of the target NNs, they are replicas of the original networks but with a slower update frequency, which allows for a more stable training of the actor and critic NNs. The update rule for soft update is given by [44]

$$\theta^{Q'} \leftarrow \tau \theta^Q + (1 - \tau) \theta^{Q'}, \quad (40a)$$

$$\theta^{\mu'} \leftarrow \tau \theta^\mu + (1 - \tau) \theta^{\mu'}, \quad (40b)$$

where $0 < \tau \ll 1$ denotes the updating rate. In accordance with the above settings, a DDPG-based TDRA algorithm is presented in Algorithm 1.

According to [45], [46], the computational complexity of the proposed DDPG-based TDRA algorithm depends on the size of the mini-batch and the NN, the number of neurons,

Algorithm 1: DDPG-based TDRA Algorithm for \mathcal{P}_1

```

1 Randomly initialize  $\mu(s; \theta^\mu)$  and  $Q(s, a; \theta^Q)$ .
  Initialize the associated target NNs with  $\theta^{\mu'} \leftarrow \theta^\mu$ ,
   $\theta^{Q'} \leftarrow \theta^Q$ .
2 Initialize the experience replay buffer  $\mathcal{B}$  with size  $M_r$ .
3 Initialize discount factor  $\beta$ , mini-batch size with  $M_b$ ,
  soft update coefficient  $\tau$ .
4 for  $episode = 1, 2, \dots, M_{ep}$  do
5   Initialize  $\mathcal{N}_n$ ,  $\mathbf{q}_S(0)$ ,  $E_S^{\max}$ ,  $\mathbf{w}_{U_k}(0)$ , and  $L_k(0)$ .
6   while  $L_k(n) > 0$  do
7     Input state  $s(n)$  into actor NN and obtain
      action  $a(n) = \mu(s(n); \theta^\mu) + \mathcal{N}_n$ .
8     Execute action  $a(n)$ , and then receive reward
       $r(n)$  and observe the next state  $s(n+1)$ .
9     Store experience tuple
       $(s(n), a(n), r(n), s(n+1))$  into  $\mathcal{B}$ .
10    if Memory counter  $> M_r$  then
11      Remove previous experience from the front
        of  $\mathcal{B}$ .
12    end
13    Randomly sample a mini-batch of  $M_b$  tuples
       $(s_i, a_i, r_i, s_{i+1})$  from  $\mathcal{B}$ .
14    Update the critic NN's weight  $\theta^Q$  by
      minimizing the critic loss function (38).
15    Update the actor NN's weight  $\theta^\mu$  according to
      (37).
16    Update the target critic NN's weight  $\theta^{Q'}$ 
      according to (40a).
17    Update the target actor NN's weight  $\theta^{\mu'}$ 
      according to (40b).
18    if  $E_S(N) \leq E_S^{\min}$  then
19      | break.
20    end
21  end
22 end

```

training steps, and the training episodes, which is expressed as $\mathcal{O}(M_{ep}NM_b \sum_{i=0}^{L-1} Z_i Z_{i+1})$, where L denotes the number of network layers and Z_i is the number of neurons in the i th layer.

IV. PERFORMANCE EVALUATION

To demonstrate the performance of the proposed DDPG-based TDRA scheme, simulation results are presented in this section. The main simulation parameters are shown in TABLE III [21], [42].

A. Network Architecture

The actor NN and critic NN employ six fully-connected neural networks, including six hidden layers with 64, 128,

TABLE III: Simulation Parameters

Parameters	Value	Parameters	Value
V_S^{\max}	20 m/s	P_k^{\max}	0.1 W
B	1 MHZ	L_k	100 Mbit
F_k^{\max}	0.1 GHZ	F_S^{\max}	20 GHZ
δ_t	0.5 s	σ_S^2, σ_E^2	-100 dBm
R_{\min}^{\sec}	0.9 Mbps	C_k, C_S	1000 cycles/bit
φ_k, φ_S	10^{-28}	$E_S^{\max} - E_S^{\min}$	20000 J
c_E	1	c_T	1
η_a	12.08	η_b	0.11
η_{Los}	1.6 dB	η_{NLoS}	23 dB
Z_{\min}	100 m	Z_{\max}	150 m
\mathbf{w}_J	$[300, 250, 0]^T$	\mathbf{q}_S^1	$[0, 250, 100]^T$
$\tilde{\mathbf{q}}_E$	$[290, 150, 100]^T$	r_E	25 m

TABLE IV: Training Parameters

Hyperparameters	Value
Total episodes M_{ep}	1000
Memory capacity M_r	10000
Mini-batch size M_b	128
Actor NN learning rate	0.0001
Critic NN learning rate	0.0006
Updating rate τ	0.001
Discount factor β	0.99
Optimizer	Adam Optimizer
κ_f	2.5×10^{-7}
κ_{ac}	1
κ_{rc}	10
ζ	10^{-7}

256, 256, 128 and 64 neurons, respectively. The activation function for all layers is the ReLU except for the output layer of the actor NN, which uses a sigmoid. It is worth noting that the states input to NN include the S 's position $\mathbf{q}_S(n)$ and the residual energy $E_S(n)$, the U_k 's achievable security rate $R_k^{\sec}(n)$ and residual data $L_k(n)$ with dimensions of 3, 1, K and K respectively. In our simulation, K is set as 5, which leads to the UAV state dimensions having a relatively small proportion within the overall state dimensions. This may need to be more effective in affecting the training process of the NN. However, $\mathbf{q}_S(n)$ and $E_S(n)$ are of great importance, and by adjusting the trajectory of S , it needs to be ensured that all the U_k 's task is processed efficiently before S runs out of energy. Thus, there exists the dimension imbalance issue, and to address it, we expand $\mathbf{q}_S(n)$ from 3 to 8 dimensions and the $E_S(n)$ from 1 to 5 dimensions to ensure that each input state dimension at one level. After dimension expansion, the input layer of the actor NN has $2K + 13$ neurons, and the critic NN has $4K + 16$ neurons. The corresponding training and reward parameters are in TABLE IV.

Due to the varying value ranges of different states, the direct input to the NN will lead to problems such as unstable training process, disappearing or exploding gradient, and difficult convergence of the model. Therefore, before inputting the state values into the NN training, each state's value needs to be normalized to $[0, 1]$ to accelerate the NN's training speed, which is implemented as follows: The state values $\{x_S(n), y_S(n), z_S(n), E_S(n), R_k^{\sec}(n), L_k(n)\}$ are divided by $\{X_{\max}, Y_{\max}, Z_{\max}, E_S^{\max}, R_{\max}^{\sec}, L_0\}$, respectively, where $(X_{\max}, Y_{\max}, Z_{\max})$ is the operation range of the UAV, and R_{\max}^{\sec} is the maximum secure offloading rate

that the user can achieve.

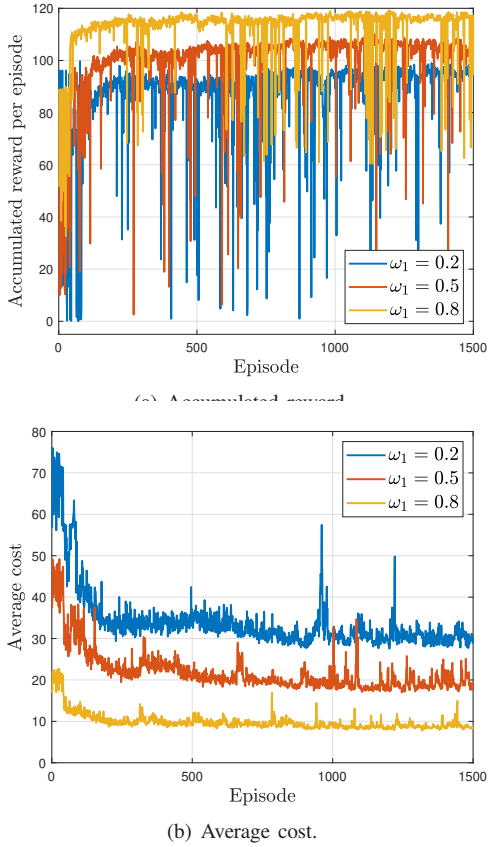
Since the output layer of the actor network uses a sigmoid activation function to scale the range of the action values to $[0, 1]$, it is necessary to scale each action value to the actual range of values. The specific implementation is as follows: the action values $\{v(n), \theta(n), \varphi(n), p_k(n), f_k(n)\}$ are multiplied by $\{V_S^{\max}, \pi, 2\pi, P_k^{\max}, F_k^{\max}\}$, respectively. In this way, by multiplying the corresponding maximum values, the standardized action values can be converted into a range of values for practical applications to ensure that the UAV and the user can operate and compute as expected.

B. Simulation Results and Analysis

To evaluate the performance of the proposed scheme, a baseline scheme is utilized as the benchmark wherein all the users offload data to S with TDMA technology. Specifically, in the benchmark scheme, the time slot is divided equally among K users, and the trajectory design, offloading strategy, and power allocation are re-implemented using the same hyperparameters as the proposed algorithm and the reward design. The TDMA-based scheme is chosen as the benchmark since it is a typical representative of the OMA scheme and was considered in many works, such as [15], [17], [19], [27]. The results of the TDMA-based scheme in this work can also provide necessary guidance and benchmarks for other OMA schemes. The instantaneous secrecy offloading rate of the benchmark scheme is expressed as

$$R_k^{\text{TDMA}, \text{sec}}(n) = \frac{B}{K} \left[\log_2 \left(1 + \frac{h_{k,S}(n) p_k(n)}{\sigma_S^2} \right) - \log_2 \left(1 + \frac{h_{k,E}^{\text{ub}}(n) p_k(n)}{h_{J,E}^{\text{lb}}(n) P_J + \sigma_E^2} \right) \right]. \quad (41)$$

Fig. 3 illustrates the accumulative reward and average cost of the proposed DDPG-based TDRA algorithm with varying ω_1 . One can find that the reward curves converge as training round increases. The accumulative reward of the proposed offloading scheme outperforms that of the benchmark scheme. This is because the proposed scheme allows multiple users to transmit data simultaneously, so the amount of data offloaded for the proposed scheme is larger than that of the benchmark scheme, which will obtain a higher offloading data reward. Furthermore, the accumulative reward of both schemes increases as ω_1 increases. This is attributed to the increasing energy cost in the average cost as ω_1 grows, resulting in the reward function primarily descending toward reducing user energy costs. Consequently, the users opt to offload more data to S , thus lowering their energy costs. Fig. 3(b) demonstrates the average cost with varying ω_1 . The average cost converges stably as training round increases. Specifically, during the initial random exploration phase, there is almost no reduction in the cost due to the higher probability of random actions, and the training will start once the replay memory buffer is filled. Moreover, the cost of the benchmark scheme begins to degrade earlier than the proposed scheme. This is because, under the same experience replay buffer size, the benchmark scheme fills the experience pool and starts training faster than NOMA because it requires longer processing time when handling the



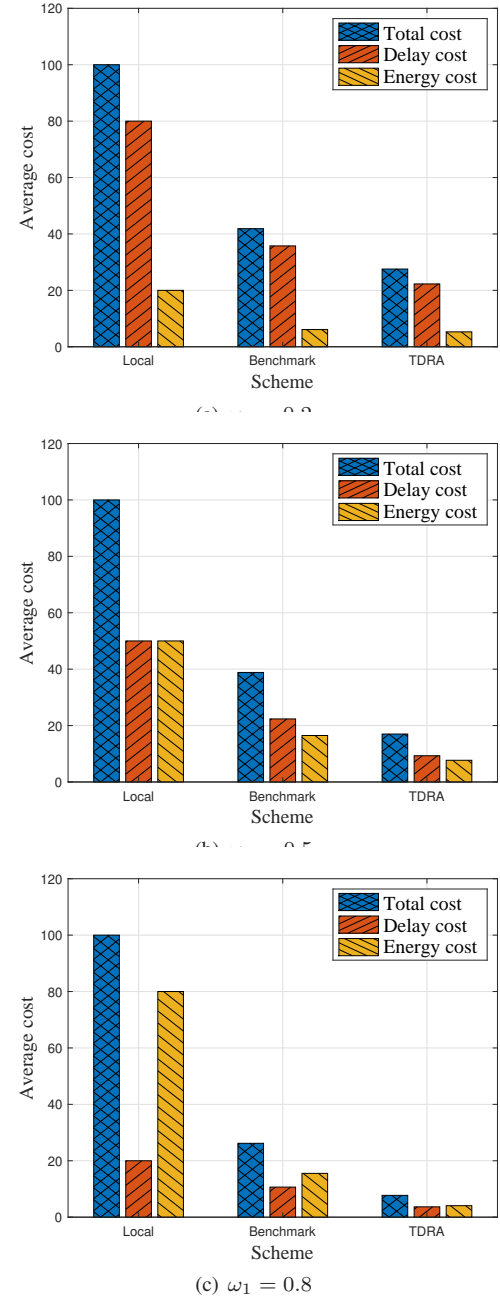
(b) Average cost.

Fig. 3: Accumulated reward and average cost with varying ω_1 .

same user data, resulting in more experiences generated in one episode for the benchmark.

Fig. 4 presents the trend of energy consumption and delay costs with varying ω_1 wherein ‘Local’ denotes that all the U_k perform all computational tasks locally with the maximum computation frequency. It can be seen that under the same weight, the cost of local scheme is the highest, followed by the benchmark, while the proposed scheme obtains the lowest average cost. This is because fully local computation processes all user data locally without the assistance of MEC servers, resulting in the highest cost while the proposed and benchmark schemes partially offload user data to S for processing, reducing the costs. In the proposed offloading scheme, users can simultaneously transmit data on the same frequency, leading to higher computational efficiency and lower average cost than the benchmark. As ω_1 increases, the proportion of energy cost in the total cost increases and the proportion of delay cost in the total cost decreases. Moreover, the average cost decreases slightly as ω_1 increases because the delay cost is higher than the energy cost when $\omega_1 = 0.5$, resulting in the total cost being more sensitive to the delay cost. Thus, by adjusting each user’s weighted factor ω_1 , a trade-off can be made between power consumption and delay.

Fig. 5 presents the optimized trajectory of S . From the overall movement trend, it can be seen that S first flies in the horizontal plane and approaches the users to improve the overall offloading rate. To obtain a lower computation cost, S

Fig. 4: The trend of energy consumption and delay costs with varying ω_1 .

flies to U_2 , who is closer to J . Due to the NOMA transmission mode, there is no need to worry about U_3 being left out. To process the data of U_4 and U_5 who are close to E , S chooses a compromise position and increases its altitude to enhance the elevation angle, thereby improving the channel gain of the $S-U_4$ and $S-U_5$ link. Additionally, different from predetermined trajectories or goal-oriented trajectories in Ref. [21], the trajectory design in this work considers the average system cost, resulting in a more convoluted path.

Fig. 6 illustrates user cost versus varying L_k . Since the data that each user can process in each slot is constant, the energy consumption and latency incurred in each slot are also stable.

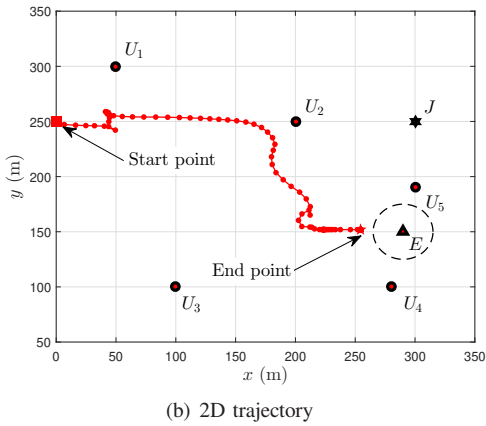
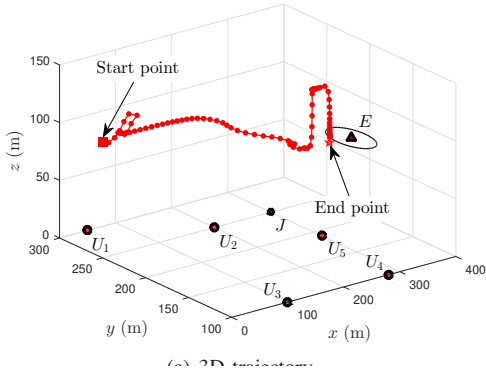


Fig. 5: The optimized trajectory.

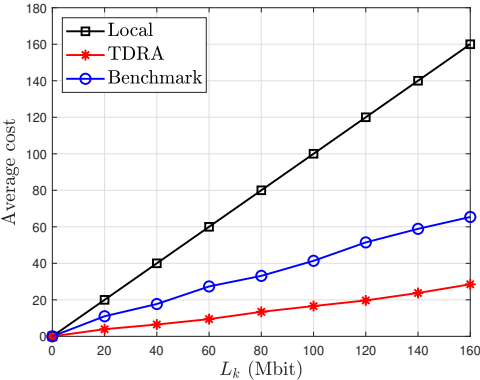


Fig. 6: The average cost with varying L_k .

As user data increases, power consumption and delay increase linearly, resulting in a linear rise in user cost. As can be seen from the figure, the costs of all three schemes increase to different degrees as L_k increases, and the larger the L_k is, the larger gap between the cost of fully local computing and the cost of offloading computing. In the lower- L_k region, the local device has the ability to process most of the data by itself, and only a small portion of the data will be offloaded to S for processing, in this case, the difference between the proposed scheme and benchmark is not obvious, and the user cost is basically equal. As increasing L_k , more data should be offloaded, the cost of the proposed scheme was reduced, which proves the efficiency of the proposed offloading scheme.

Fig. 7 describes the average cost with varying R_{\min}^{\sec} and r_E .

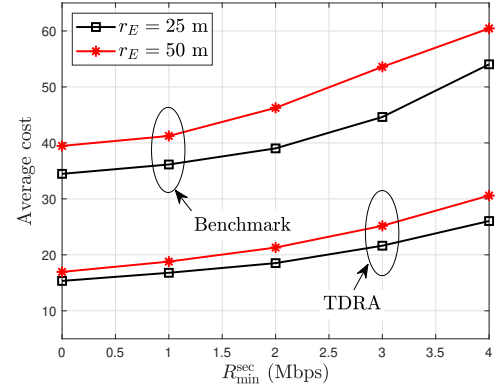


Fig. 7: The average cost with varying R_{\min}^{\sec} and r_E .

One can observe that as R_{\min}^{\sec} increases, the average cost also increases. This is attributed to the high R_{\min}^{\sec} , which denotes more stringent condition for user offloading, resulting in a decrease of the data offloaded by users, with more data being processed locally. Moreover, larger r_E results in large cost. This is because larger r_E signifies the higher uncertainty of the eavesdropper information in the considered system.

V. CONCLUSION

In this work, security offloading in a NOMA-based multi-user UAV-MEC system has been investigated. A novel optimization problem was formulated involving the concurrent design of the 3D trajectory, user transmission power, and CPU frequency to minimize the average computational cost. A DDPG-based TDRA scheme was proposed to address the optimization challenge posed by high-dimensional continuous action space control in this scenario, aiming to achieve efficient user resource allocation and flight trajectory design of the UAV. The simulation results confirmed that the proposed DDPG-based TDRA algorithm can effectively solve the secure offloading challenges posed by uncertain eavesdropping locations. Considering the scenarios with multiple UAVs and multiple terrestrial random-roaming or directional-walking users will be part of future work.

REFERENCES

- [1] N. Abbas, Y. Zhang, A. Taherkordi, and T. Skeie, "Mobile edge computing: A survey," *IEEE Internet Things J.*, vol. 5, no. 1, pp. 450-465, Feb. 2018.
- [2] P. Mach and Z. Becvar, "Mobile edge computing: A survey on architecture and computation offloading," *IEEE Commun. Surv. Tutor.*, vol. 19, no. 3, pp. 1628-1656, 3rd Quart., 2017.
- [3] Y. Ye, L. Shi, X. Chu, R. Q. Hu, and G. Lu, "Resource allocation in backscatter-assisted wireless powered MEC networks with limited MEC computation capacity," *IEEE Trans. Wireless Commun.*, vol. 21, no. 12, pp. 10678-10694, Dec. 2022.
- [4] Y. Zeng, R. Zhang, and T. J. Lim, "Wireless communications with unmanned aerial vehicles: Opportunities and challenges," *IEEE Commun. Mag.*, vol. 54, no. 5, pp. 36-42, May. 2016.
- [5] Q. Hu, Y. Cai, G. Yu, Z. Qin, M. Zhao, and G. Y. Li, "Joint offloading and trajectory design for UAV-enabled mobile edge computing systems," *IEEE Internet Things J.*, vol. 6, no. 2, pp. 1879-1892, Apr. 2019.
- [6] Y. Liu, K. Xiong, Q. Ni, P. Y. Fan, and K. Ben Letaief, "UAV-assisted wireless powered cooperative mobile edge computing: Joint offloading, CPU control, and trajectory optimization," *IEEE Internet Things J.*, vol. 7, no. 4, pp. 2777-2790, Apr. 2020.

[7] C. Sun, W. Ni, and X. Wang, "Joint computation offloading and trajectory planning for UAV-assisted edge computing," *IEEE Trans. Wireless Commun.*, vol. 20, no. 8, pp. 5343-5358, Aug. 2021.

[8] B. Liu, Y. Wan, F. Zhou, Q. Wu, and R. Q. Hu, "Resource allocation and trajectory design for MISO UAV-assisted MEC networks," *IEEE Trans. Veh. Technol.*, vol. 71, no. 5, pp. 4933-4948, May. 2022.

[9] Y. Xu, T. Zhang, Y. Liu, D. Yang, L. Xiao, and M. Tao, "UAV-assisted MEC networks with aerial and ground cooperation," *IEEE Trans. Wireless Commun.*, vol. 20, no. 12, pp. 7712-7727, Dec. 2021.

[10] Z. Hu, F. Zeng, Z. Xiao, B. Fu, H. Jiang, H. Xiong, Y. Zhu, and M. Alazab, "Joint resources allocation and 3D trajectory optimization for UAV-enabled space-air-ground integrated networks," *IEEE Trans. Veh. Technol.*, vol. 72, no. 11, pp. 14214-14229, Nov. 2023.

[11] J. Ji, K. Zhu, C. Yi, and D. Niyato, "Energy consumption minimization in UAV-assisted mobile-edge computing systems: Joint resource allocation and trajectory design," *IEEE Internet Things J.*, vol. 8, no. 10, pp. 8570-8584, May. 2021.

[12] I. Budhiraja, N. Kumar, S. Tyagi, and S. Tanwar, "Energy consumption minimization scheme for NOMA-based mobile edge computation networks underlaying UAV," *IEEE Syst. J.*, vol. 15, no. 4, pp. 5724-5733, Dec. 2021.

[13] X. Zhang, J. Zhang, J. Xiong, L. Zhou, and J. Wei, "Energy-efficient multi-UAV-enabled multiaccess edge computing incorporating NOMA," *IEEE Internet Things J.*, vol. 7, no. 6, pp. 5613-5627, Jun. 2020.

[14] W. Feng, J. Tang, N. Zhao, X. Zhang, X. Wang, K.-K. Wong, and J. A. Chambers, "Hybrid beamforming design and resource allocation for UAV-aided wireless-powered mobile edge computing networks with NOMA," *IEEE J. Sel. Areas Commun.*, vol. 39, no. 11, pp. 3271-3286, Nov. 2021.

[15] Y. Xu, T. Zhang, D. Yang, Y. Liu, and M. Tao, "Joint resource and trajectory optimization for security in UAV-assisted MEC systems," *IEEE Trans. Commun.*, vol. 69, no. 1, pp. 573-588, Jan. 2021.

[16] P. Chen, X. Luo, D. Guo, Y. Sun, J. Xie, Y. Zhao, and R. Zhou, "Secure task offloading for MEC-aided-UAV system," *IEEE Trans. Intell. Veh.*, vol. 8, no. 5, pp. 3444-3457, May. 2023.

[17] W. Mao, K. Xiong, Y. Lu, P. Fan, and Z. Ding, "Energy consumption minimization in secure multi-antenna UAV-assisted MEC networks with channel uncertainty," *IEEE Trans. Wireless Commun.*, vol. 22, no. 11, pp. 7185-7200, Nov. 2023.

[18] Y. Zhou, C. Pan, P. L. Yeoh, K. Wang, M. Elkashlan, B. Vucetic, and Y. Li, "Secure communications for UAV-enabled mobile edge computing systems," *IEEE Trans. Commun.*, vol. 68, no. 1, pp. 376-388, Jan. 2020.

[19] W. Lu, Y. Ding, Y. Gao, S. Hu, Y. Wu, N. Zhao, and Y. Gong, "Resource and trajectory optimization for secure communications in dual-UAV-MEC systems," *IEEE Trans. Ind. Informat.*, vol. 18, no. 4, pp. 2704-2713, Apr. 2022.

[20] Y. Ding, H. Han, W. Lu, Y. Wang, N. Zhao, X. Wang, and X. Yang, "DDQN-based trajectory and resource optimization for UAV-aided MEC secure communications," *IEEE Trans. Veh. Technol.*, vol. 73, no. 4, pp. 6006-6011, Apr. 2024.

[21] W. Lu, Y. Ding, Y. Gao, Y. Chen, N. Zhao, Z. Ding, and A. Nallanathan, "Secure NOMA-based UAV-MEC network towards a flying eavesdropper," *IEEE Trans. Commun.*, vol. 70, no. 5, pp. 3364-3376, May. 2022.

[22] H. Yang, S. Liu, L. Xiao, Y. Zhang, Z. Xiong, and W. Zhuang, "Learning-based reliable and secure transmission for UAV-RIS-assisted communication systems," *IEEE Trans. Wireless Commun.*, vol. 23, no. 7, pp. 6954-6967, Jul. 2024.

[23] H. Yang, K.-Y. Lam, L. Xiao, Z. Xiong, H. Hu, D. Niyato, and H. Vincent Poor, "Lead federated neuromorphic learning for wireless edge artificial intelligence," *Nature Commun.*, vol. 13, no. 1, Jul. 2022.

[24] N. Lin, H. Tang, L. Zhao, S. Wan, A. Hawbani, and M. Guizani, "A PDDQNL algorithm for energy efficient computation offloading in UAV-assisted MEC," *IEEE Trans. Wireless Commun.*, vol. 22, no. 12, pp. 8876-8890, Dec. 2023.

[25] L. Wang, K. Wang, C. Pan, W. Xu, N. Aslam, and A. Nallanathan, "Deep reinforcement learning based dynamic trajectory control for UAV-assisted mobile edge computing," *IEEE Trans. Mobile Comput.*, vol. 21, no. 10, pp. 3536-3550, Oct. 2022.

[26] Y. He, Y. Gan, H. Cui, and M. Guizani, "Fairness-based 3-D multi-UAV trajectory optimization in multi-UAV-assisted MEC system," *IEEE Internet Things J.*, vol. 10, no. 13, pp. 11383-11395, Jul. 2023.

[27] R. Zhao, J. Xia, Z. Zhao, S. Lai, L. Fan, and D. Li, "Green MEC networks design under UAV attack: A deep reinforcement learning approach," *IEEE Trans. Green Commun. Netw.*, vol. 5, no. 3, pp. 1248-1258, Sept. 2021.

[28] W. Lu, Y. Mo, Y. Feng, Y. Gao, N. Zhao, Y. Wu, and A. Nallanathan, "Secure transmission for multi-UAV-assisted mobile edge computing based on reinforcement learning," *IEEE Trans. Netw. Sci. Eng.*, vol. 10, no. 3, pp. 1270-1282, May. 2023.

[29] Q. Wu, Y. Zeng, and R. Zhang, "Joint trajectory and communication design for multi-UAV enabled wireless networks," *IEEE Trans. Wireless Commun.*, vol. 17, no. 3, pp. 2109-2121, Mar. 2018.

[30] H. Lei, C. Zhu, K.-H. Park, W. Lei, I. S. Ansari, and T. A. Tsiftsis, "On secure NOMA-based terrestrial and aerial IoT systems," *IEEE Internet Things J.*, vol. 9, no. 7, pp. 5329-5343, Apr. 2022.

[31] A. Al-Hourani, S. Kandeepan, and S. Lardner, "Optimal LAP altitude for maximum coverage," *IEEE Wireless Commun. Lett.*, vol. 3, no. 6, pp. 569-572, Dec. 2014.

[32] H. Lei, X. Wu, K.-H. Park, and G. Pan, "Joint 3D trajectory and user scheduling for energy constrained aerial IoT systems under probabilistic LoS channel," *arXiv:2406.01313*, Jun. 2024, [Online]: <https://arxiv.org/abs/2406.01313>.

[33] R. Zhong, X. Liu, Y. Liu, and Y. Chen, "Multi-agent reinforcement learning in NOMA-aided UAV networks for cellular offloading," *IEEE Trans. Wireless Commun.*, vol. 21, no. 3, pp. 1498-1512, Mar. 2022.

[34] Z. Shi, X. Xie, H. Lu, H. Yang, J. Cai, and Z. Ding, "Deep reinforcement learning-based multidimensional resource management for energy harvesting cognitive NOMA communications," *IEEE Trans. Commun.*, vol. 70, no. 5, pp. 3110-3125, May. 2022.

[35] Z. Shi, X. Xie, H. Lu, H. Yang, and J. Cai, "Deep reinforcement learning based dynamic user access and decode order selection for uplink NOMA system with imperfect SIC," *IEEE Wireless Commun. Lett.*, vol. 10, no. 4, pp. 710-714, Apr. 2021.

[36] H. Lei, F. Yang, I. S. Ansari, H. Liu, K. J. Kim, and T. A. Tsiftsis, "Secrecy outage performance analysis for uplink CR-NOMA systems with hybrid SIC," *IEEE Internet Things J.*, vol. 10, no. 15, pp. 13181-13195, Aug. 2023.

[37] L. Lv, F. Zhou, J. Chen, and N. Al-Dhahir, "Secure cooperative communications with an untrusted relay: A NOMA-inspired jamming and relaying approach," *IEEE Trans. Inf. Forensics Security*, vol. 14, no. 12, pp. 3191-3205, Dec. 2019.

[38] H. Lei, H. Yang, K.-H. Park, I. S. Ansari, J. Jiang, and M.-S. Alouini, "Joint trajectory design and user scheduling for secure aerial underlay IoT systems," *IEEE Internet Things J.*, vol. 10, no. 15, pp. 13637-13648, Aug. 2023.

[39] S. Liu, Y. Yu, L. Guo, P. L. Yeoh, B. Vucetic, Y. Li, and T. Q. Duong, "Satisfaction-maximized secure computation offloading in multi-eavesdropper MEC networks," *IEEE Trans. Wireless Commun.*, vol. 21, no. 6, pp. 4227-4241, Jun. 2022.

[40] Y. Zeng, J. Xu, and R. Zhang, "Energy minimization for wireless communication with rotary-wing UAV," *IEEE Trans. Wireless Commun.*, vol. 18, no. 4, pp. 2329-2345, Apr. 2019.

[41] Z. Yang, W. Xu, and M. Shikh-Bahaei, "Energy efficient UAV communication with energy harvesting," *IEEE Trans. Veh. Technol.*, vol. 69, no. 2, pp. 1913-1927, Feb. 2020.

[42] R. Ding, F. Gao, and X. S. Shen, "3D UAV trajectory design and frequency band allocation for energy-efficient and fair communication: A deep reinforcement learning approach," *IEEE Trans. Wireless Commun.*, vol. 19, no. 12, pp. 7796-7809, Dec. 2020.

[43] H. Lei, H. Ran, I. S. Ansari, K.-H. Park, G. Pan, and M.-S. Alouini, "DDPG-based aerial secure data collection," *IEEE Trans. Commun.*, vol. 72, no. 8, pp. 5179-5193, Aug. 2024.

[44] D. Silver, G. Lever, N. Heess, T. Degris, D. Wierstra, and M. Riedmiller, "Deterministic policy gradient algorithms," in *Proc. Int. Conf. Mach. Learn. (ICML)*, Beijing, Jun. 2014, pp. 387-395.

[45] K. D. Wang, H. D. Li, Z. G. Ding, and P. Xiao, "Reinforcement learning based latency minimization in secure NOMA-MEC systems with hybrid," *IEEE Trans. Wireless Commun.*, vol. 22, no. 1, pp. 408-422, Jan. 2023.

[46] H. Yang, Z. Xiong, J. Zhao, D. Niyato, L. Xiao, and Q. Wu, "Deep reinforcement learning-based intelligent reflecting surface for secure wireless communications," *IEEE Trans. Wireless Commun.*, vol. 20, no. 1, pp. 375-388, Jan. 2021.